Applied Surface Science 254 (2008) 5261–5265

Contents lists available at ScienceDirect

Applied Surface Science

journal homepage: www.elsevier.com/locate/apsusc

Growth mechanism and characterisation of chemically grown Sb doped Bi_2Se_3 thin films

N.S. Patil [a], A.M. Sargar [b], S.R. Mane [b], P.N. Bhosale [b,*]

[a] Kisan Shikshan Sanstha's Krantisinh Nana Patil College, Walwa 416313, District: Sangli, India
[b] Materials Research Laboratory, Department of Chemistry, Shivaji University, Kolhapur 416004, India

ARTICLE INFO

Article history:
Received 15 June 2007
Received in revised form 12 February 2008
Accepted 14 February 2008
Available online 29 February 2008

Keywords:
Thin Films
$Bi_{2-x}Sb_xSe_3$
XRD
SEM

ABSTRACT

The synthesis of combinatorial $Bi_{2-x}Sb_xSe_3$ thin films by arrested precipitation technique (APT) using triethanolamine-bismuth, triethanolamine-antimony and sodium selenosulphite as sources of Bi^{3+}, Sb^{3+} and Se^{2-}, respectively is investigated on commercial glass substrates. The growth mechanism of film formation, composition and surface morphology of the as deposited films were studied as a function of preparative parameters and bath composition. The films were monophasic, polycrystalline and covered the surface of the substrate completely. Energy dispersive X-ray analysis gave coherent elemental composition indicating single phase $BiSbSe_3$ was made. The good results obtained for $Bi_{2-x}Sb_xSe_3$ thin films revealed that arrested precipitation technique is best suited for the deposition of large area thin films on conducting/nonconducting substrates to produce materials for device applications.

1. Introduction

The best materials for thermoelectric application at room temperature were V_2VI_3 compounds and their alloy because of high thermoelectric figure of merit. $Bi_{2-x}Sb_x$ alloys are very attractive materials for thermoelectric refrigeration at low temperature using Ettingshausen effect [1,2].

Thin films of bismuth–antimony chalcogenides find many applications such as thermoelectric power generator, thermoelectric refrigerator, thermopile detector, effective sensing and controlling of temperature at localized areas such as microelectronic or optoelectronic devices etc. [3–6]. In order to increase the thermoelectric efficiency, extensive studies on Bi_2Te_3 doping have been carried out by many researchers [7,8]. Patil et al. [9] and Damodara Das et al. [10] reported preparation and properties of V_2VI_3 group chalcogenide thin films and their mixed/alloyed combinations. In the present investigation, we have deposited Sb doped Bi_2Se_3 thin films using modified chemical bath deposition known as arrested precipitation technique (APT) [11,12]. To the best of our knowledge nobody has reported stoichiometric $Bi_{2-x}Sb_xSe_3$ films by arrested precipitation technique. Hence it is our interest to study the details of growth procedure and relevant properties of $Bi_{2-x}Sb_xSe_3$ thin films. The present paper is purposing to analyze the change in the growth mechanism, optical, structural and morphological properties of $Bi_{2-x}Sb_xSe_3$ thin films, induced by the doping of Sb. The doping of Sb impurity was confirmed from the energy dispersive X-ray analysis (EDS) analysis.

2. Experimental details

$Bi_{2-x}Sb_xSe_3$ thin films were deposited on to the chemomechanically and ultrasonically cleaned glass substrate using APT. Equimolar Bi–TEA, Sb–TEA and Na_2SeSO_3 were used as basic source materials.

UV–visible spectrophotometer (Hitachi model 330, Japan) was used to determine absorption spectra of $Bi_{2-x}Sb_xSe_3$ in the wavelength range 350–850 nm. The layer thickness of the as deposited samples was measured by gravimetric technique using highly sensitive electronic balance; Mettler Toledo GmbHCH-8606 Greifensee having an accuracy of ±0.01 mg. The absorption coefficient, band gap and type of transition were determined from these studies. X-ray diffraction (XRD) analysis was carried out using a Philips PW-1710 X-ray diffractometer for the 2θ ranging from 0° to 100° with Cu Kα line used as a beam (λ = 1.5418A°). Scanning electron microscopy (SEM) and energy dispersive X-ray analysis was performed on a JEOL-JSM- 6360A scanning microscope.

* Corresponding author. Tel.: +91 231 2609338.
E-mail address: p_n_bhosale@rediffmail.com (P.N. Bhosale).

0169-4332/$ – see front matter © 2008 Elsevier B.V. All rights reserved.
doi:10.1016/j.apsusc.2008.02.084

3. Results and discussion

3.1. Growth mechanism

The novel structural behaviour and properties of thin films can largely be ascribed to their growth process which is therefore of basic importance to the science and technology of thin films. The detail of nucleation and growth depends on the material being deposited and other parameters such as nature of substrate, temperature and pH. In the present investigation we have slightly modified the chemical deposition method using polydentate chelating agent, triethanolamine [$N(CH_2–CH_2–OH)_3$] as a complexing agent to arrest Bi^{3+} and Sb^{3+} ions. The APT is based on Ostwald ripening law. According to this law if metal ions in solution are arrested using polydentate complexing agent, the rate of reaction between metal ions and chalcogen ions can be well controlled to get desired quality of metal chalcogenide thin films.

The stability constant indicates strong affinity of the organic complexing agent TEA towards Bi^{3+} and Sb^{3+} ions and its tendency to keep the Bi^{3+} and Sb^{3+} ions arrested in a solution even in alkaline pH range where the metal hydroxide formation is possible. Concentration of precursors also shows strong influence on the growth of Bi_2Se_3 and mixed/alloyed $Bi_{2-x}Sb_xSe_3$ thin films, therefore concentration of the precursors was taken in the ratio 2:3. In the present investigation ionic species of Bi^{3+}, Sb^{3+} and Se^{2-} are produced as per the following reaction equilibria in an aqueous alkaline deposition bath.

$$(NH_4)_3[Bi2N(CH_2-CH_2-O)_3] + 6H_2O \xrightarrow{pH10} Bi^{3+} + 3NH_4OH + 3OH^- + 2[N(CH_2-CH_2-OH)_3] \quad (1)$$

$$(NH_4)_3[Sb2N(CH_2-CH_2-O)_3] + 6H_2O \xrightarrow{pH10} Sb^{3+} + 3NH_4OH + 3OH^- + 2N(CH_2-CH_2-OH)_3 \quad (2)$$

$$Na_2SeSO_3 + OH^- \rightarrow Na_2SO_4 + HSe^- \qquad HSe^- + OH^- \rightarrow H_2O + Se^{2-} \quad (3)$$

The reactions (1) and (2) show that the metal ions are produced by dissociation of the metal complex while chalcogen ions are produced by dissociation of sodium selenosulphite. At pH 10 ± 0.2 the ionic product of Bi^{3+}, Sb^{3+} and Se^{2-} ions exceeds the solubility product of $Bi_{2-x}Sb_xSe_3$ in the reaction bath, which results in ion by ion condensation of growth of bismuth antimony selenide thin films on substrate support as per reaction,

$$Bi^{3+}_{2-x} + Sb^{3+}_{x} + 3Se^{2-} \rightarrow Bi_{2-x}Sb_xSe_3$$

$Bi_{2-x}Sb_xSe_3$ films prepared by arrested precipitation technique are found to be uniform and adhere tightly to the substrate support.

3.2. Optical studies

Measurements of absorbance in $Bi_{2-x}Sb_xSe_3$ chalcogenide thin films in the wavelength region 350–850 nm at room temperature were carried out. The optical absorption coefficient (α) of $Bi_{2-x}Sb_xSe_3$ with different compositions was calculated using the absorbance value measured for a particular wavelength (λ) and film thickness (t). Thickness of the film was calculated by assuming density of the film is equal to bulk material. The optical absorption coefficient is found to be in the order of 10^4 cm^{-1}. The optical band gap was found graphically from the calculated values of the absorption coefficient (α).

In semiconductors, the optical absorption spectrum has been found to have three distinct regions

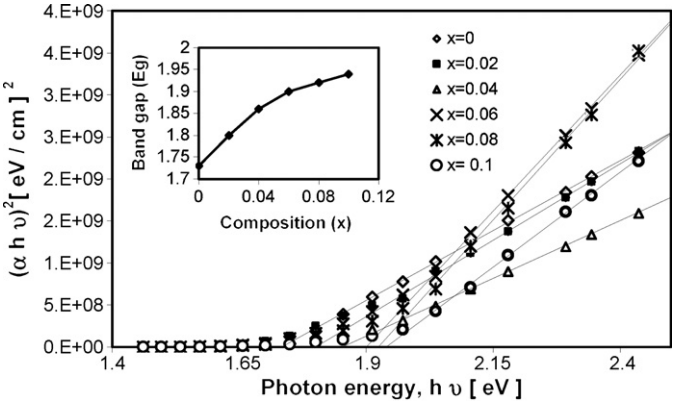

Fig. 1. The $(\alpha h\nu)^2$ versus $h\nu$ plots for the $Bi_{2-x}Sb_xSe_3$ films having different compositions.

(i) High absorption region ($\alpha \geq 10^4$ cm^{-1}),
(ii) exponential edge region ($1 \leq \alpha \geq 10^4$ cm^{-1}),
(iii) weak absorption tail ($1 \leq \alpha$ cm^{-1}).

At higher wavelengths the non-linear tail absorption in the curves may be due to transitions associated with the absorption of longer wavelength phonons. In the high absorption region ($\alpha \geq 10^4$ cm^{-1}), the relation between the absorption coefficient (α) and the incident photon energy ($h\nu$) can be written as [13]

$$(\alpha h\nu)^{1/n} = A(h\nu - E_g)$$

where 'h' is Planck's constant, 'ν' is frequency, 'A' is parameter that depends on the transition probability and 'E_g' is the optical energy gap of the investigated sample and exponent 'n' depends on the type of transition. For direct allowed $n = 1/2$, indirect allowed transition $n = 2$, and for direct forbidden $n = 3/2$. The values of the optical band gap have been calculated from the best straight line fits in '$(\alpha h\nu)^{1/n}$' versus '$h\nu$' plots and corresponding band gaps were obtained from extrapolating the straight portion of the graph on '$h\nu$' axis at $\alpha = 0$.

Fig. 1 shows the plot '$(\alpha h\nu)^2$' versus '$h\nu$', i.e. with $n = 1/2$ for the films of $Bi_{2-x}Sb_xSe_3$. The presence of single slope in the curves suggests that films are of single phase in nature and the type of transition is direct and allowed. It was found that the optical energy gap E_g increases gradually from 1.73 to 1.94 eV with increasing Sb mole content (x) up to 0.1. The calculated values of the optical energy gap were plotted versus Sb content as shown in inset of Fig. 1. The rate of change of the optical gap decreases as the Sb content increases. The increase of band gap with Sb doping concentration is related with the decrease of particle size which is evidenced in the XRD pattern (Fig. 3) and SEM micrograph (Fig. 4) [14,15]. Most of the published results on the optical properties of bismuth selenide are based on the optical reflectance on single crystals of Bi_2Se_3 with relatively high electrical conductivities [16,17]. These results cannot be readily correlated with the present work. The difference in the optical band gap between the bulk value and thin film values arises from the quantum confinement of charge carriers. Lack of crystallinity or vary small grain size (nanometer size) could shift the band gap to higher values compared with the bulk crystalline value [18]. The optical band gap derived for each film is listed in Table 1. The mode of optical transition has also been determined by plotting $\ln(\alpha h\nu)$ versus $\ln(h\nu - E_g)$. According to Bhattacharya et al. [19], $\ln(\alpha h\nu)$ versus $\ln(h\nu - E_g)$ variation should give a straight line with a slope equal to 0.5 for a direct allowed type of transition. In our case, the above variations are straight line with a slope of nearly 0.5 for all compositions confirming the allowed direct transitions as shown

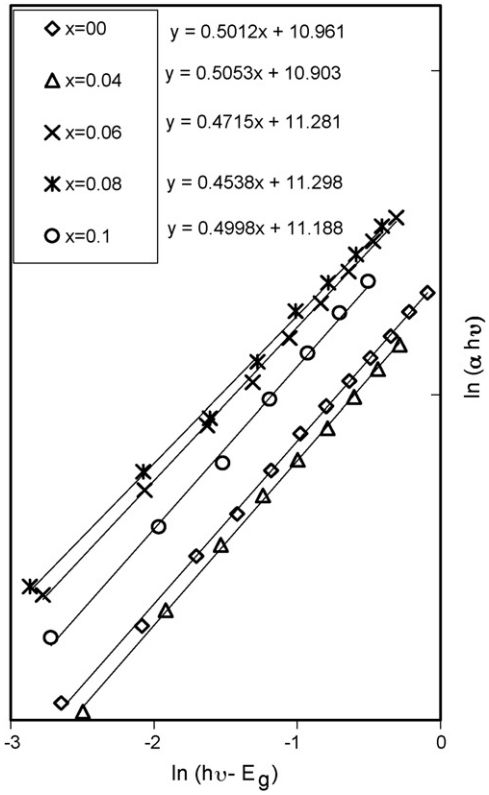

Fig. 2. Evolution of the mode of transition from the variation of $\ln(\alpha h\nu)$ versus $\ln(h\nu - E_g)$ for $Bi_{2-x}Sb_xSe_3$ samples.

Table 1
Composition parameter dependent properties of $Bi_{2-x}Sb_xSe_3$ thin films

$Bi_{2-x}Sb_xSe_3$ film composition (x)	Band gap (E_g)	Power factor (n)
0	1.73	0.5012
0.02	1.80	–
0.04	1.86	0.5053
0.06	1.90	0.4715
0.08	1.92	0.4538
0.10	1.94	0.4998

in Fig. 2. The values of slopes obtained from $\ln(\alpha h\nu)$ versus $\ln(h\nu - E_g)$ plots are listed in Table 1.

3.3. XRD studies

Fig. 3 is the XRD pattern of $Bi_{2-x}Sb_xSe_3$ with various Sb contents (x = 0, 0.02, 0.04, 0.06, 0.08, 0.1) deposited at 45 °C. The peaks become broader and some peaks appeared at high θ values with increasing Sb doping. This is conclusive evidence for new ordering. Careful observation on the pattern of the deposits shows that some lines were remained unchanged in the pattern and some new lines appeared in the pattern. The increase in the number of lines is not due to improvement in the crystallinity but due to introduction of new plane spacings, caused by nonuniform distortion as a result of doping. There are no JCPDS standard data available for different compositions of $Bi_{2-x}Sb_xSe_3$. Hence the plane indices are obtained by comparing the intensities and positions of the peaks with those of Bi_2Se_3 and Sb_2Se_3 which are given by JCPDS file no. 77-2016 and 15-0861. The formation of solid solution is expected because both materials crystallises in orthorhombic structure. Table 2 lists the observed 'd' values for Bi_2Se_3 and $Bi_{2-x}Sb_xSe_3$ thin films in comparison with the JCPDS data. The observed 'd' values are in good agreement with the standard values for the orthorhombic

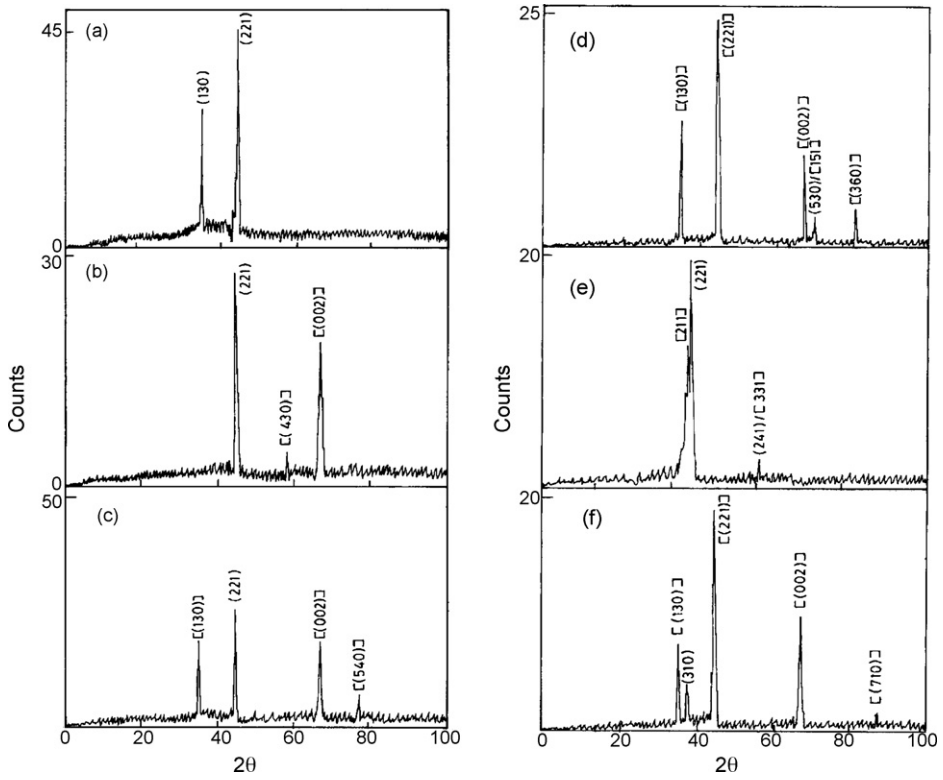

Fig. 3. X-ray diffractograms of six typical $Bi_{2-x}Sb_xSe_3$ samples having different compositions (x): (a) 0, (b) 0.02, (c) 0.04, (d) 0.06, (e) 0.08, (f) 0.10.

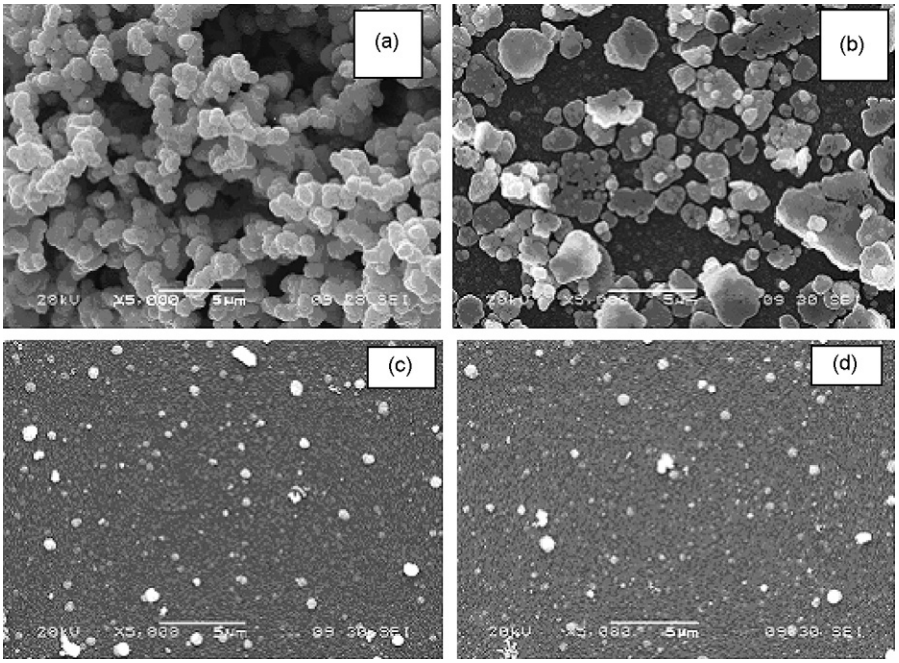

Fig. 4. SEM micrographs for $Bi_{2-x}Sb_xSe_3$ films: (a) $x = 0$, (b) $x = 0.02$, (c) $x = 0.06$, (d) $x = 0.1$.

structure of Bi_2Se_3 and Sb_2Se_3. The strongest peak for all films occurred at $2\theta = 44.8^\circ$ with $d = 2.9A^\circ$ (corresponding to (2 2 1) reflection). It indicates that the preferred orientation lies along (2 2 1) direction for $Bi_{2-x}Sb_xSe_3$ thin films deposited by APT. Furthermore, the intensity of the (2 2 1) peak decreases and small peak broadening occurs with an increase of Sb content. This small degree of broadening occurs as a result of increase in strain in the film due to Sb incorporation in the Bi lattice site. This indicates that the crystal quality decreases with an increase of Sb content in the film. The crystalline size (grain diameter), D, of the deposits was calculated using the Scherrer formula [20] for the (2 2 1) peak assuming that microstrain can be neglected

$$D = \frac{k\lambda}{\beta \cos\theta}$$

where, k constant varies with $h\ k\ l$ and crystallite shape but usually nearly equal to 0.9, λ wavelength of source radiation, β full-width at half maximum of the peak, in radian, θ Bragg angle.

The crystallite size decreases from 35.8 to 18.7 nm with increasing Sb doping as shown in Table 3.

Table 2
XRD results of Bi_2Se_3 and $Bi_{2-x}Sb_xSe_3$ thin films

Film composition	JCPDS 'd' values Å Bi_2Se_3			JCPDS 'd' values Å Sb_2Se_3			Observed 'd' values in Å	
	'd' (Å)	($h\ k\ l$)	Intensity	'd' (Å)	[$h\ k\ l$]	Intensity	'd' (Å)	Intensity (%)
Bi_2Se_3	3.7341	(1 3 0)	67.5	–	–	–	3.7707	37.1
	2.9112	(2 2 1)	92.5	–	–	–	3.0024	100
$Bi_{1.98}Sb_{.02}Se_3$	2.9112	(2 2 1)	92.5	–	–	–	3.0005	100
	2.3388	(4 3 0)	30.2	2.337	[4 3 0]	14	2.3836	22.0
	2.045	(0 0 2)	41.5	1.989	[0 0 2]	25	2.0749	42.6
$Bi_{1.96}Sb_{.04}Se_3$	3.7341	(1 3 0)	67.5	3.72	[1 3 0]	30	3.7868	45.4
	2.9112	(2 2 1)	92.5	–	–	–	3.0021	100
	2.0450	(0 0 2)	41.5	1.989	[0 0 2]	25	2.0711	48.7
	1.8273	(5 4 0)	3.7	1.826	[5 4 0]	4	1.8302	14.9
$Bi_{1.94}Sb_{.06}Se_3$	3.7341	(1 3 0)	67.5	3.72	[1 3 0]	30	3.7728	66.8
	2.9112	(2 2 1)	92.5	–	–	–	3.0021	100
	2.0450	(0 0 2)	41.5	1.989	[0 0 2]	25	2.0700	37.2
	2.0021	(5 3 0)	17.4	1.998	[1 5 1]	25	1.9976	12.5
	1.7556	(3 6 0)	7.0	1.752	[3 6 0]	20	1.7669	14.3
$Bi_{1.92}Sb_{.08}Se_3$	–	–	–	3.162	[2 1 1]	75	3.0997	60.5
	2.9112	(2 2 1)	92.5	–	–	–	3.0030	100
	2.2155	(2 4 1)	13.0	2.268	[3 3 1]	8	2.2529	13.7
$Bi_{1.90}Sb_{.1}Se_3$	3.7341	(1 3 0)	67.5	3.72	[1 3 0]	30	3.7779	46.5
	3.6810	(3 1 0)	49.0	–	–	–	3.5593	14.3
	2.9112	(2 2 1)	92.5	–	–	–	3.0046	100
	2.0450	(0 0 2)	41.5	1.989	[0 0 2]	25	2.0672	46.5
	1.6438	(7 1 0)	1.7	1.646	[7 1 0]	6	1.6448	16.5
	1.6202	(6 4 0)	4.9	1.619	[6 4 0]	6	1.6217	23.5

Table 3
The grain size (D) and half peak width (β) of the $Bi_{2-x}Sb_xSe_3$ films

Film composition	Crystalline size 'D' (nm)	Half peak width 'β' (radian)
Bi_2Se_3	35.789	0.004189
$Bi_{1.98}Sb_{.02}Se_3$	28.634	0.005237
$Bi_{1.96}Sb_{.04}Se_3$	24.541	0.006109
$Bi_{1.94}Sb_{.06}Se_3$	20.451	0.007331
$Bi_{1.92}Sb_{.08}Se_3$	18.672	0.008030
$Bi_{1.90}Sb_{.1}Se_3$	17.892	0.008379

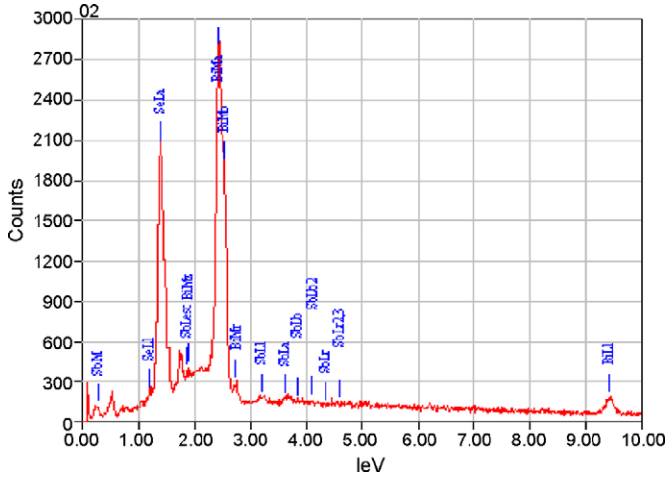

Fig. 5. The EDS scanning pattern of the as deposited $Bi_{1.94}Sb_{0.06}Se_3$ thin film.

3.4. SEM and EDS studies

Fig. 4(a–d) shows scanning electron micrograph of top view of the four typical $Bi_{2-x}Sb_xSe_3$ thin films in the as-grown condition at 5000× magnification. The SEM micrographs show well adherent, smooth and uniform film surface without cracks under low magnification which accounts high mechanical stability of the sample [19]. We have observed significant variation in the morphological properties of the films for the variation of Sb doping.

Fig. 4a represents the surface morphology of the Bi_2Se_3 thin film, which shows cross-linked spherical grains of uniform size spread all over the surface. Some regions of overgrowth were also observed. After doping Sb slightly ($x = 0.02$), cross-linked grains coalesce and aggregates of crystallites are formed as shown in Fig. 4b. It shows the co-existence of small and relatively large grains on the film surface. Fig. 4c and d shows that large crystallites are broken to well defined nanocrystalline particles with fine background as a result of further antimony doping. These micrographs reveal that the grain size decreases as the result of increase in Sb doping indicating that Sb is grain growth inhibitor in $Bi_{2-x}Se_3$ films. The grain size of the $Bi_{2-x}Sb_xSe_3$ films with $x = 0$, 0.02, 0.04, 0.06, 0.1 are 970, 560 to 890, 240 to 560 and 160 to 560 nm, respectively. These results are consistent with the XRD results which also show broadening of peaks as a result of antimony doping indicating decrease of crystalline size. Surface morphology of the films remains almost same after doping concentration $x \geq 0.06$.

The quantitative analysis by energy dispersive X-ray analysis was performed for Bi, Sb and Se in $Bi_{2-x}Sb_xSe_3$ samples at different points. Fig. 5 displays an EDS spectrum of typical $Bi_{1.94}Sb_{.06}Se_3$ and elemental compositional analysis of a series of the as deposited $Bi_{2-x}Sb_xSe_3$ samples is listed in Table 4 showing that samples are in good stoichiometric ratio. Chemical compositions of both small and bigger grains are found to be same and ruled out the segregation of any specific element.

Table 4
EDS analysis of the as deposited $Bi_{2-x}Sb_xSe_3$ thin films

Film composition	Elements (expected at %)			Elements (actual at %)		
	Bi	Sb	Se	Bi	Sb	Se
$Bi_{1.96}Sb_{.04}Se_3$	39.20	0.80	60	44.24	0.82	54.94
$Bi_{1.94}Sb_{.06}Se_3$	38.80	1.20	60	43.35	1.23	55.42
$Bi_{1.90}Sb_{.10}Se_3$	38.00	2.00	60	43.43	2.06	54.51

4. Conclusions

In conclusion, this communication demonstrates that polycrystalline $Bi_{2-x}Sb_xSe_3$ thin films have been successfully, in a simple way, synthesized using APT at low temperature. The films are mechanically stable. Optical measurement revealed a band gap tailoring when Sb doping in the film is varied. The preferred orientation lies along the [2 2 1] direction. This work should prove useful in understanding the roles of Sb doping in controlling the final morphologies of polycrystalline materials.

Acknowledgements

One of the authors (NSP) is indebted to University Grants Commission, New Delhi (India) for sanction of teacher fellowship for Ph.D. work. The author is also thankful to Kisan Shikshn Sanstha's Krantisinh Nana Patil College, Walwa for supporting this work.

References

[1] H.J. Goldsmid, Br. J. Appl. Phys. 14 (1963) 271–274.
[2] M.P.R. Panicker, M. Mc Knaster, F.A. Kroger, J. Electrochem. Soc. 125 (1978) 566.
[3] D.B. Hyun, J.S. Hwang, T.S. Oh, J.D. Shim, N.V. Kolomoets, J. Phys. Chem. Solids 59 (1998) 1039.
[4] J. Yang, T. Aizawa, A. Yamamoto, T. Ohta, Mater. Chem. Phys. 70 (2001) 90–94.
[5] N.G. Patel, P.G. Patel, Solid State Electrochem. 35 (1992) 1269.
[6] Il-ho Kim, Mater. Lett. 44 (2000) 75–79.
[7] K. Tittes, A. Bund, W. Plieth, A. Bentien, S. Paschen, M. Plotner, H. Grafe, W.-J. Fischer, J. Solid State Electrochem. 7 (2003) 714.
[8] W. Wang, Q.H. Huang, F.L. Jia, J. Zhu, J. Appl. Phys. 96 (2004) 615.
[9] A.R. Patil, V.N. Patil, M.A. Anuse, P.N. Bhosale, L.P. Deshmukh, Thin Solid Films 414 (2002) 155–162.
[10] V. Damodara Das, P. Gopal Ganeshan, Mater. Chem. Phys. 57 (1998) 57–66.
[11] B.D. Ajalkar, R.K. Mane, B.D. Sarwade, P.N. Bhosale, Solar Energy Mater. Solar Cells 81 (2004) 101–112.
[12] R.K. Mane, B.D. Ajalkar, P.N. Bhosale, Mater. Chem. Phys. 82 (2003) 534–537.
[13] in: J.I. Penkove (Ed.), Optical Processes in Semiconductors. Prentice-Hall, Inc. (1971) p. 34.
[14] V.M. Garcia, M.T.S. Nair, P.K. Nair, R.A. Zingaro, Semicond. Sci. Technol. 12 (1997) 645.
[15] Sk.F. Ahmed, S. Khan, P.K. Ghosh, M.K. Mitra, K.K. Chattopadhyay, J. Sol–Gel Sci. Technol. 39 (2006) 241–247.
[16] V.V. Sobolev, V.M. Kramer, S.G. Kozlova, G.L. Temchuk, Sov. Phys. Semicond. 23 (1990) 889.
[17] M. Stordeur, K.K. Ketavong, A. Priemuth, H. Sobotta, V. Riede, Phys. Status Solidi b 169 (1992) 505.
[18] L. Huang, P.K. Nair, M.T.S. Nair, R.A. Zingaro, E.A. Mayers, Thin Sold Films 268 (1995) 49–56.
[19] D. Bhattacharya, S. Chaudhuri, A.K. Pal, Vacuum 43 (1992) 313.
[20] V. Bilgin, I. Akyuz, S. Kose, F. Atay, Semicond. Sci. Technol. 21 (2006) 579–585.